Motion-Induced Directionality of Collective Emission in a Nonchiral Waveguide

Yoan Spahn,[1] Jens Hartmann,[2] Benedikt Saalfrank,[1] Michael Fleischhauer,[2]
Thomas Halfmann,[1] and Thorsten Peters[1]
[1]Institute of Applied Physics, Technical University of Darmstadt, Hochschulstraße 6, 64289 Darmstadt, Germany
[2]Department of Physics and Research Center OPTIMAS, RPTU University Kaiserslautern-Landau, 67663 Kaiserslautern, Germany

(Received 12 March 2026; accepted 17 August 2026; published 14 September 2026)

We report the experimental observation of motion-induced directionality in collective atomic emission within a hollow-core waveguide, establishing a general principle: directional interactions can emerge from collective phase engineering alone. Remarkably, neither single-emitter asymmetry nor any asymmetry in the geometric arrangement of the system is required—both the atom-field coupling and the spontaneous emission are fully isotropic in our system. Instead, Raman-induced effective two-level emitters with spatially oscillating transition dipole phases and atomic motion give rise to controllable directionality, reaching values up to 0.89(1). We study the correlations of the superfluorescent bursts close to and well above the threshold to collective emission; we find thermal statistics below and a buildup of coherence above it. Numerical simulations based on the truncated Wigner approximation for spins yield good agreement. Additionally we present a simple model based on position uncertainty capable of reproducing the observed directionality. Our results open a new route to directional interactions in nonchiral systems, with direct implications for the design of directional metamaterials and photonic structures built from isotropic constituents.

DOI: 10.1103/9dhz-dxc8

Understanding and controlling coupling in light-matter interfaces is one of the main goals of quantum optics. A basic setting involves the emission of photons by an ensemble of emitters. In dilute ensembles, the interaction of quantum emitters with vacuum fluctuations of the radiation field creates oscillating atomic dipoles with random phase, leading to isotropic spontaneous emission of light and exponential decay. This is quite different in dense [1–4] or waveguide-coupled ensembles [5–8]. Here, dissipative dipole-dipole couplings mediated by photon exchange synchronize the atomic dipoles and modify the emission process. As a consequence, collective scattering in the form of superradiant light bursts [1,2] can emerge with nonexponential decay and a preferred bidirectional emission along the axis of largest optical depth. By coupling the emitters to a chiral interface [9,10], as, e.g., realized by photonic nanostructures [11–13] or chiral arrangement of individual emitters [14,15], even unidirectional emission can be achieved. These interfaces have seen increased interest in recent years as they give rise to nonreciprocal interactions [16–20] with applications for, e.g., photonic metamaterials [21], nanophotonics [22–25], magnonics [26], and many-body systems [27]. There, unidirectional guiding occurs at the level of single emitters or due to their spatial arrangement and, thus, also affects collective emission [7].

We here report the first experimental observation of collective emission from a disordered ensemble with controllable directionality in a *nonchiral* one-dimensional (1D) waveguide. Contrary to [28], there is no random spontaneous symmetry breaking. Figures 1(d)–1(f) show three examples of the detected normalized light power emitted in forward (+) and backward (−) directions for different maximum cooperation numbers N_{mc} and velocity spread σ_{v} (defined below). We clearly notice a strong asymmetry depending on the ratio of collective decay to motional timescale indicated by the box color, although there is no chiral coupling or special spatial arrangement of individual emitters. As we show by comparison with numerical simulations, the directionality, only emerging in the collective dynamics, is caused by an interplay between atomic motion and the fact that the quantum emitters are effective two-level systems created in a Raman process [see Fig. 1(a)]. While the preferred direction is determined by the excitation geometry, the directionality itself is induced by atomic motion and requires a finite velocity spread. Directional Raman amplification in waveguide-coupled atomic ensembles has been discussed in [29,30]; there, however, the directionality relies on chiral light-matter coupling.

Published by the American Physical Society under the terms of the Creative Commons Attribution 4.0 International license. Further distribution of this work must maintain attribution to the author(s) and the published article's title, journal citation, and DOI.

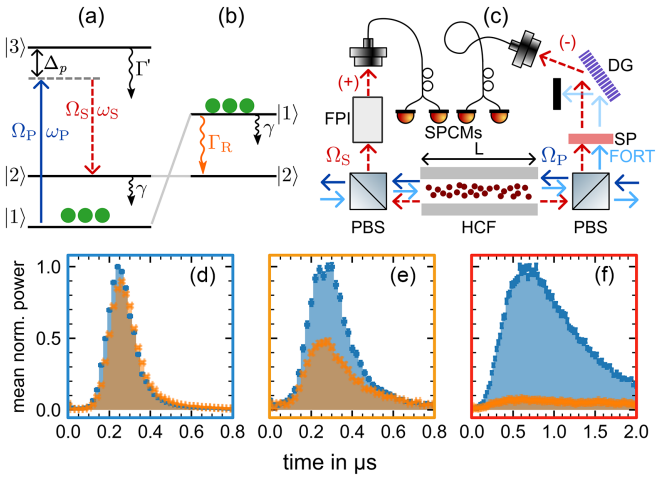


FIG. 1. Simplified three-level system of ^{87}Rb (a) with $|1\rangle, |2\rangle, |3\rangle \doteq {}^2S_{1/2}F = 1, {}^2S_{1/2}F = 2, {}^2P_{1/2}F' = 2$ that corresponds to an effective two-level system (b) for pump detuning $\Delta_p \gg \Gamma'$ of decay rate $\Gamma = \Gamma_R \propto \Omega_p^2$ with pump Rabi frequency Ω_p. (c) Simplified experimental setup. (d)–(f) Experimental examples for superfluorescent bursts measured in (+) (blue) and (−) direction (orange) for $(\sigma_v; N_{mc})$ of $(1.5; 160)$ (d), $(1.5; 106)$ (e), and $(5; 132)$ (f).

Figure 1(c) depicts our experimental setup (for details, see Refs. [8,31]). We load up to $N = 2 \times 10^5$ laser-cooled ^{87}Rb atoms from a magneto-optical trap into a hollow-core fiber [HCF, NKT Photonics, HC-800-02, core diameter 7(1) μm, NA = 0.092(6)] where they are guided by an optical far-off-resonant trap (FORT) in running-wave configuration [31]. Inside the HCF, the atomic ensemble has a temperature $T = 1.1(1)$ mK and a near Gaussian radial density profile of $1/e$ radius $\sigma_a \sim 1.7$ μm, similar to the $1/e^2$ intensity mode radius $\sigma_p \sim 2.75$ μm of the laser beams. To avoid perturbing AC Stark shifts by the FORT during the measurements, we switch it periodically off and on, providing measurement windows of $\tau_m = 2.5$ μs, during which the ensemble is freely expanding (see Supplemental Material [32]). Before each measurement, we prepare the ensemble in the lower ground state $|1\rangle$ by optical pumping. We then send a pump pulse of power P_p, detuned by $\Delta_p = 26.4\Gamma'$ from transition $|1\rangle \leftrightarrow |3\rangle$, into the HCF, which induces spontaneous Raman scattering to state $|2\rangle$ at a rate $\Gamma_R \propto P_p/\Delta_p^2$. This creates an effective inverted two-level system $\{|1\rangle, |2\rangle\}$ [8] [see Figs. 1(a) and 1(b)] with a dipole moment carrying a spatially oscillating phase factor $\sim e^{ik_p z}$ and a single-atom decay rate $\Gamma = \Gamma_R$ tunable via P. Here, the inversion arises naturally from the Raman process itself.

The long-range coupling provided by the HCF lets collective scattering build up at the Stokes transition $|2\rangle \rightarrow |3\rangle$, leading to the emission of superfluorescent (SF) bursts. Since not all N atoms contribute to collective scattering, we determine a maximum cooperation number $N_{mc}^{(\pm)} = \eta_s \eta_{inh} \mu N$, taking into account the limited coupling of spontaneous radiation into each of the (±) HCF modes ($\mu = NA^2/4$), as well as spatial (η_s) and spectral inhomogeneities (η_{inh}) due to pump attenuation and AC Stark shifts by the pump [8]. This yields $N_{mc}^{(\pm)} \lesssim 150$ effective collective emitters for each direction, resulting in a total $N_{mc} = 2N_{mc}^{(\pm)}$ (see Supplemental Material [32]). By tuning Γ via the pump power P_p, we control the relative (thermal) velocity distribution width $\sigma_v = \bar{v}/(\lambda_0 \Gamma)$ of the ensemble, where $\bar{v}$ is the rms thermal velocity and λ_0 is the transition wavelength of the effective two-level system. The ratio of collective emission to motional dephasing timescale is $R_\tau = \tau_{col}/\tau_{th} = 2\sigma_v/N_{mc}$, with the thermal dephasing time $\tau_{th} = \lambda/\bar{v}$ and the characteristic superradiant time $\tau_{col} = 2/N_{mc}\Gamma$, neglecting directionality. For varying σ_v and N_{mc}, we measure the light exiting the HCF in the (±) directions, detected by a set of four single-photon counting modules (SPCMs, Excelitas, SPCM-AQRH-13) in a double Hanbury-Brown Twiss (HBT) configuration, followed by a time-tagging device (Swabian Instruments, TimeTagger 20). Measurement protocols used to extract the relative (±) burst amplitudes are given in Supplemental Material [32].

We first investigate the pulse dynamics and correlations of the emitted bursts. Figure 2 shows the intensity profiles and the two-time correlation function $g^{(2)}(t_1, t_2)$ for light emitted into the (+) direction well above [Figs. 2(a) and 2(b)] and close to the threshold to SF emission [Figs. 2(c) and 2(d)]. We calculate the second-order correlation function $g^{(2)}(t_1, t_2) = \langle N_1(t_1) N_2(t_2)\rangle / [\langle N_1(t_1)\rangle \langle N_2(t_2)\rangle]$ from the measured count rates N_i of the ith SPCM. We apply averaging over different single experimental realizations. In Figs. 2(a) and 2(b), the correlations are thermal with $g^{(2)}(t,t) \approx 2$ during the initial stages of the SF bursts, where the dynamics is determined by vacuum fluctuations. As the bursts build up, $g^{(2)}(t,t)$ decreases, indicating a buildup of coherence due to the synchronization of dipoles as observed and discussed in [37,38]. The minimum $g^{(2)}(t,t) = 1.31(5)$ occurs shortly after the burst maximum; thereafter $g^{(2)}(t,t) \rightarrow 2$, indicating a loss of coherence. This is consistent with the Dicke model, where the peak emission rate is reached when the population distribution between the initial and final state is equal, and the coherence is maximal [1,2]. The deviation from $g^{(2)}(t,t)$ reaching unity is expected for our extended sample and enhanced by shot-to-shot fluctuations of the burst delay inherent to the SF process. For conditions close to the SF threshold [Figs. 2(c) and 2(d)], in contrast, $g^{(2)}(t,t) = 1.8(3)$, i.e., always close to the thermal value. As the emitted pulse is 1.5 times longer than in Figs. 2(a) and 2(b) and obeys thermal statistics, we interpret this as amplified spontaneous emission [39]. We observe a smooth transition approaching the threshold, showing an increase

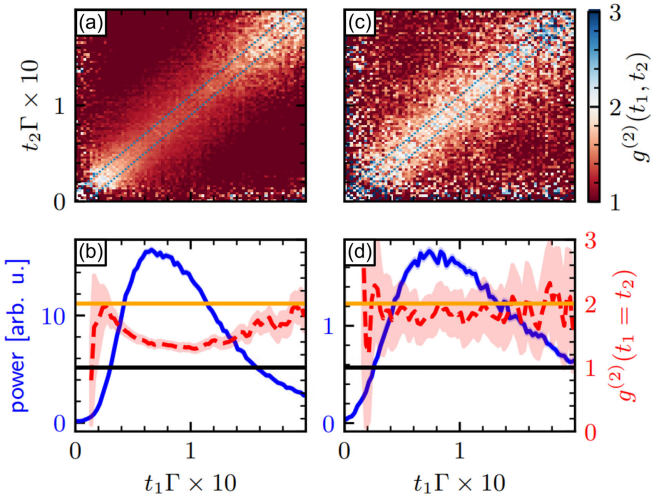


FIG. 2. Temporal evolution of the pulse power and correlation functions above (a),(b) and close to the SF threshold (c),(d) for $N_{mc} = 248(7)$ and $N_{mc} = 55(6)$, respectively. Two-time autocorrelation functions $g^{(2)}(t_1, t_2)$ are shown in (a),(c) with the corresponding average count rates (blue) during the bursts along with the equal time $g^{(2)}(t, t)$ (red, dashed). Intervals used for averaging $g^{(2)}(t, t)$ are marked by blue dotted lines in (a),(c). Measured at $\Gamma = 2\pi \times 18.1(6)$ kHz, and averaged over 20×10^3 (a), (b) and 50×10^3 (c),(d) realizations.

in the minimal value of $g^{(2)}(t, t) \to 2$. Measurements further below the threshold did not change the SF dynamics qualitatively but resulted in worse statistics. The backward emission showed the same behavior. The cross-correlation between the $(+/-)$ directions is close to unity except during the burst buildup (see Fig. S5 in Supplemental Material [32]).

To understand the experimental results, we employ numerical simulations based on the truncated Wigner approximation (TWA) for a spatially extended ensemble of spins [40]. Collective light emission from an ensemble of atoms can be described by an effective spin model [41–44], obtained by integrating over the reservoir degrees of freedom of the light field. Here, the density matrix ϱ of the spins obeys a Lindblad master equation, $\dot{\varrho} = -i[H, \varrho] + \mathcal{L}\varrho$, with effective Hamiltonian H and Lindblad operator $\mathcal{L}$,

$$H = \frac{1}{2}\sum_{l,m} J_{lm}\sigma_l^+\sigma_m^-, \tag{1}$$

$$\mathcal{L}\varrho = \frac{1}{2}\sum_{l,m} \Gamma_{lm}(\sigma_l^+\sigma_m^-\varrho + \varrho\sigma_l^+\sigma_m^- - 2\sigma_m^-\varrho\sigma_l^+), \tag{2}$$

where $\Gamma_{lm} \sim \mathrm{Re}[\vec{d}_l^* \cdot \mathbf{G}(z_l, z_m, \omega_0) \cdot \vec{d}_m]$ describes the strength of the collective decay process and $J_{lm} \sim \mathrm{Im}[\vec{d}_l^* \cdot \mathbf{G}(z_l, z_m, \omega_0) \cdot \vec{d}_m]$ describes the dipole-dipole exchange interaction. $\vec{d}_m$ is the dipole matrix element of the atom at position z_m, and $\mathbf{G}(z_l, z_m, \omega_0)$ is the Green's tensor of the radiation field at the transition frequency ω_0 [41]. In a 1D system, the collective coupling reads $\Gamma_{lm} = \Gamma_{1D}(\beta_+ e^{ik_0 z_{lm}} + \beta_- e^{-ik_0 z_{lm}})$ and $J_{lm} = i\Gamma_{1D}/2(\beta_+ e^{ik_0|z_{lm}|} - \beta_- e^{-ik_0|z_{lm}|})$, where the coefficients $\beta_\pm$ account for a potential chiral coupling of a single emitter to the waveguide; see, e.g., [7,45,46]. If $\beta_+ = \beta_- = \frac{1}{2}$, there is full inversion symmetry between the forward and backward direction. Γ_{1D} is the single-atom emission rate into the waveguide, $k_0 = \omega_0/c$, and $z_{lm} = z_l - z_m$ is the relative position of the atoms, which is time dependent due to atomic motion. Additionally, we add single-atom decay with rate Γ in Eq. (2). The complex field amplitude emitted in $(\pm)$ direction of the waveguide at the two ends is then a sum over emission contributions of all spins, $E_\pm = i\sqrt{(\Gamma_{1D}/2)}\sum_j e^{i(k_p \mp k_0)z_j}\sigma_j^-$, with $k_p = \omega_p/c$.

We numerically simulate the effective spin model, Eqs. (1) and (2), using the TWA for spins [40,47] and the collective correspondence rules [40], which have proven to give accurate predictions of superradiance in waveguide systems [46]. The stochastic method is numerically inexpensive and allows for the simulation of up to several thousand interacting spins (details in Supplemental Material [32]). As the total number of atoms $N \sim 10^5$ in the experiment is larger, a straightforward simulation is computationally too costly. We, thus, theoretically investigate a reduced system with a much smaller number of emitters $N_{mc} \sim 300$ as in the experiment. We compensate this by assuming stronger coupling $\Gamma'_{1D} = \Gamma$ to the waveguide mode, while keeping the cooperativity $N_{mc}\Gamma'_{1D} = N\Gamma_{1D}$ the same. This clearly underestimates the effect of spontaneous emission events into nonwaveguide modes in the simulation and other single-atom effects as dephasing and, thus, does not allow us to accurately describe the behavior near or below the threshold of SF emission. Above this threshold, the simulations of the reduced model do, however, reproduce the experimental results rather well for the temporal evolution of the burst power (blue) as well as the correlations (red) shown in Fig. 3(a). We observe qualitative agreement for all parameters in collective decay. Only the timescale, measured by the pulse widths in Fig. 3(b), is slightly larger than the experimental values. However, both experiment and simulation exhibit similar (antiproportional) scaling between N_{mc} and τ_{FWHM}.

We now turn to the directionality of the SF emission shown in Figs. 1(d)–1(f). To measure it precisely, we change the direction of the pump beam instead of using differing detection ports (see Supplemental Material [32]). We quantify the directionality by $\kappa = (R_+ - R_-)/(R_+ + R_-)$, where $R_\pm$ are the peak photon rates in $(\pm)$ direction. The experimental dependence of κ on N_{mc} is shown in Fig. 4(a) for three different values of the velocity spread σ_v (in units of $\lambda_0\Gamma$). In each measurement, directionality decreases for low N_{mc}, i.e., $\kappa \to 0$ for $N_{mc} \to 0$. Fully symmetric emission can be seen for the two lowest σ_v

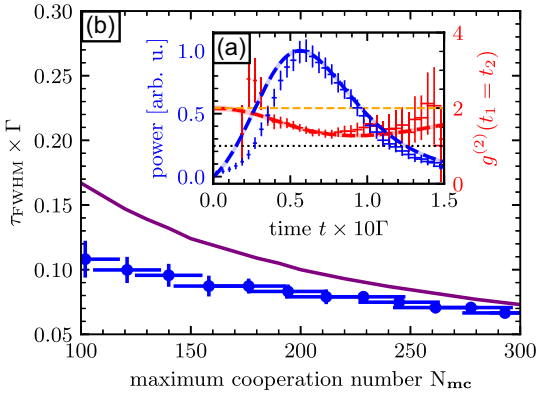


FIG. 3. (a) Emitted optical power vs time (blue) and equal time $g^{(2)}(t,t)$ (red) vs N_{mc} in (+) direction for $N = 71(6) \times 10^3$ (corresponding to $N_{\mathrm{mc}} = 280$) and $\Gamma = 2\pi \times 33(2)$ kHz, averaged over 56×10^3 realizations. Dashed lines show TWA simulations, while data points show measurement results. Horizontal lines indicate thermal (orange) and coherent (black) correlations. (b) Experimental SF burst widths (blue symbols) vs N_{mc} for $\Gamma = 2\pi \times 33(2)$ kHz. The purple line shows the results of full numerical calculations averaged over 5×10^4 trajectories.

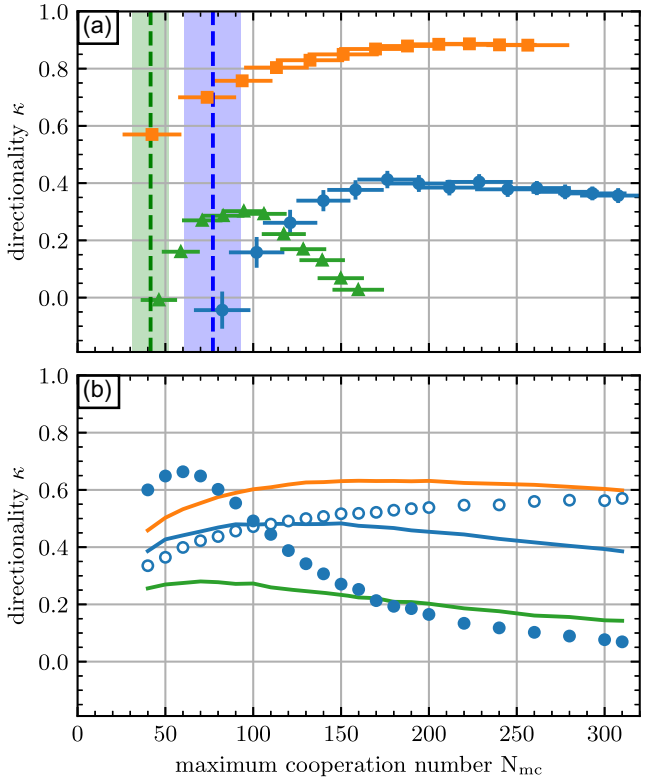


FIG. 4. (a) Measured directionality κ (symbols) of the SF burst amplitudes in (±) direction vs N_{mc}. The pump power was set to three different values at $\Delta_p = 26.4\Gamma_{D_1}$ corresponding to $\Gamma/(2\pi) = 20(2)$ kHz, 33(2) kHz, and 67(2) kHz. This results in σ_{v} of 5.0(2) (orange squares), 3.0(1) (blue circles), and 1.50(2) (green triangles), respectively. The vertical lines indicate the SF thresholds. (b) Corresponding κ as obtained from the TWA simulations including motion (lines). The results of the static effective model (see End Matter) for $\sigma_{\mathrm{v}} = 3$ are shown by symbols, assuming constant τ (open circles) as well as $\tau(N_{\mathrm{mc}}) = (N_{\mathrm{mc}}\Gamma/2)^{-1}$ (full circles). Each data point was averaged over 5×10^4 trajectories, resulting in uncertainties smaller than the symbol size.

(green, blue). For the largest σ_{v} (orange), we were not able to reach sufficiently small N_{mc}, resulting in a minimal κ of 0.58(1). With increasing N_{mc}, κ first increases toward a maximum, before decreasing again for further increasing N_{mc}. The $\sigma_{\mathrm{v}} = 5$ data extend only slightly beyond this maximum so that the already weak decline appears as a plateau. For the maximal N_{mc} available in our experiment, κ approaches zero only for the smallest σ_{v} (green triangles). A decrease for large N_{mc} is seen in all measurements, however. Figure 4(b) shows the results of the simulations. Most importantly, we took atomic motion during the emission process into account, assuming a Maxwell-Boltzmann distribution of velocities with width σ_{v} as determined from experimental data. Without atomic motion, the simulations yield $\kappa = 0$; including it indeed results in a nonuniform collective emission in (+) and (−) direction with $\kappa > 0$. The simulations reproduce the same behavior as described for the experimental data. In particular, they show κ rising to a maximum before decreasing with N_{mc}. The regimes $N_{\mathrm{mc}} \to 0$ and $N_{\mathrm{mc}} \to \infty$, in which symmetric emission is recovered, are not theoretically accessible. We only observe good quantitative agreement far in the collective regime for $\sigma_{\mathrm{v}} = 3$ (blue); otherwise, the simulations yield only reasonable qualitative agreement, for the following reasons. For small N_{mc}, the increase in κ reflects the interplay between purely spontaneous emission and the emergence of collective emission beyond the threshold. As argued before, the model used in the simulation with smaller atom number N_{mc} yields only a faithful representation of collective effects but strongly underestimates spontaneous and amplified spontaneous emission below threshold. Hence, disagreement at low N_{mc} is to be expected. Furthermore, the maximum directionality is amplified by the difference in SF thresholds, an effect not correctly represented in the full simulations. This becomes more relevant when the threshold difference is large, i.e., at large σ_{v}. Finally, the simulations neglect the Stokes gain of the ensemble [8], which also contributes to the directionality and can account for deviations of up to 7% (see Supplemental Material [32]). Given the strong simplifications of the model, a precise quantitative agreement cannot be expected. However, the qualitative dependencies of κ on both N_{mc} and σ_{v} are well described by it.

We argue that the directionality and its dependence on N_{mc} and σ_{v} is due to motional-induced dephasing and the fact that the dipole transition matrix elements of the dressed two-level system [see Fig. 1(a)] have a space-dependent phase. To this end, we use a static model (see End Matter for details) mapping motion onto location uncertainty

via an undetermined mapping factor τ. As we can see in Fig. 4(b), such a static model requires a N_{mc}-dependent mapping factor to qualitatively reproduce the nonmonotonicity of the full simulations (full circles).

We, thus, interpret our findings as follows. Below the threshold to collective decay {vertical lines in Fig. 4(a); see Supplemental Material [32]}, the emission results from incoherent, (amplified) spontaneous decay and exhibits no directionality. Note that at the lowest P_p ($\sigma_{\mathrm{v}} = 5$) no clear threshold toward the SF regime could be determined because the transition is less sharp. Once the threshold is crossed, collective effects become significant, and directionality in (+) direction arises. In the collective regime, the ratio of collective to motional timescale R_τ provides a qualitative guide to the behavior of κ. If R_τ increases, the collective processes slow down compared to thermal motion, and the resulting dephasing yields stronger directionality. This can be achieved by decreasing N_{mc} or increasing σ_{v}. Vice versa, increasing N_{mc} results in decreasing directionality deep in the collective regime. Depending on σ_{v}, more or less collective emitters are required to counteract the thermal dephasing. Only for the smallest $\sigma_{\mathrm{v}} = 1.5$ do we reach the regime where the collective dynamics outpaces motional dephasing and the emission becomes symmetrical again.

Additionally, the maximal directionality near the SF threshold is increased by the fact that the threshold in the (−) direction is at slightly higher N_{mc} than in the (+) direction due to the additional decoherence introduced by two-photon Doppler broadening, estimated as $\approx 0.2\Gamma'$. The resulting larger threshold difference gives a stronger increase of κ, increasing the maximum directionality up to $\kappa = 0.89(1)$. We can, thus, easily tune the collective emission directionality in our system by the pump power and atom number, i.e., the collective decay rate.

In summary, we have given clear experimental evidence of an emergent directionality of SF collective emission in a *nonchiral* waveguide, tunable by the ratio of the collective emission rate to the rate of motional dephasing. The experimental observations are in fair qualitative agreement with full-scale numerical TWA simulations if the motion of atoms during the emission process is taken into account. They are qualitatively understood by replacing atomic motion by a localization uncertainty of atoms at rest. For the directionality to occur, a breaking of the $(+/-)$ symmetry is needed, provided here by the pump laser parallel to the fiber axis. Excitation of the elongated ensemble from any other angle—not perpendicular to the HCF—would also give motion-induced directional emission. Similar directional collective emission could be observed without a pump laser in a thermal ensemble of initially inverted two-level emitters whose dipole moment has a spatially oscillating phase. Our Letter identified a new mechanism of emerging directionality of collective radiative couplings in a system with fully isotropic emitters. Besides being of fundamental interest, we anticipate applications in photonics [48,49], waveguide QED [33], and new ways to realize directional interactions in quantum optical systems [16–20] using isotropic building blocks and collective phase engineering.

Acknowledgments—This work was funded by the Deutsche Forschungsgemeinschaft (DFG, German Research Foundation, Project No. 410249930) and SFB/TR 185 (Project No. 277625399).

Y. S. and B. S. conducted and evaluated the experiment, J. H. performed the TWA simulations, and the static model was developed by M. F. T. P. supervised the experiment with support of T. H. M. F. supervised the theoretical work. All authors contributed to the discussion of the results and the writing of the manuscript.

Data availability—The data used for this work are available from the authors upon reasonable request.

[1] R. H. Dicke, Phys. Rev. **93**, 99 (1954).
[2] M. Gross and S. Haroche, Phys. Rep. **93**, 301 (1982).
[3] N. E. Rehler and J. H. Eberly, Phys. Rev. A **3**, 1735 (1971).
[4] G. Ferioli, A. Glicenstein, F. Robicheaux, R. T. Sutherland, A. Browaeys, and I. Ferrier-Barbut, Phys. Rev. Lett. **127**, 243602 (2021).
[5] P. Solano, J. A. Grover, J. E. Hoffman, S. Ravets, F. K. Fatemi, L. A. Orozco, and S. L. Rolston, in *Advances in Atomic, Molecular, and Optical Physics* (Elsevier, New York, 2017), Vol. 66, pp. 439–505.
[6] R. Pennetta, M. Blaha, A. Johnson, D. Lechner, P. Schneeweiss, J. Volz, and A. Rauschenbeutel, Phys. Rev. Lett. **128**, 073601 (2022).
[7] C. Liedl, F. Tebbenjohanns, C. Bach, S. Pucher, A. Rauschenbeutel, and P. Schneeweiss, Phys. Rev. X **14**, 011020 (2024).
[8] S. Stryzhenko, A. Bruns, and T. Peters, Phys. Rev. Res. **6**, 013091 (2024).
[9] P. Lodahl, S. Mahmoodian, S. Stobbe, A. Rauschenbeutel, P. Schneeweiss, J. Volz, H. Pichler, and P. Zoller, Nature (London) **541**, 473 (2017).
[10] D. G. Suárez-Forero, M. Jalali Mehrabad, C. Vega, A. González-Tudela, and M. Hafezi, PRX Quantum **6**, 020101 (2025).
[11] J. Petersen, J. Volz, and A. Rauschenbeutel, Science **346**, 67 (2014).
[12] O. A. Iversen and T. Pohl, Phys. Rev. Lett. **126**, 083605 (2021).
[13] Q. Miao and G. S. Agarwal, Phys. Rev. Res. **7**, 013138 (2025).
[14] J. S. Peter, S. Ostermann, and S. F. Yelin, Phys. Rev. Res. **6**, 023200 (2024).
[15] M. L. Xavier, F. A. Pinheiro, and R. Bachelard, arXiv:2602.15231.
[16] M. Fruchart, R. Hanai, P. B. Littlewood, and V. Vitelli, Nature (London) **592**, 363 (2021).
[17] C. Caloz, A. Alù, S. Tretyakov, D. Sounas, K. Achouri, and Z.-L. Deck-Léger, Phys. Rev. Appl. **10**, 047001 (2018).

[18] S. V. Kutsaev, A. Krasnok, S. N. Romanenko, A. Y. Smirnov, K. Taletski, and V. P. Yakovlev, Adv. Photonics Res. **2**, 2000104 (2021).
[19] N. Nefedkin, M. Cotrufo, A. Krasnok, and A. Alù, Adv. Quantum Technol. **5**, 2100112 (2022).
[20] T. Nadolny, C. Bruder, and M. Brunelli, Phys. Rev. X **15**, 011010 (2025).
[21] E. Galiffi, R. Tirole, S. Yin, H. Li, S. Vezzoli, P. A. Huidobro, M. G. Silveirinha, R. Sapienza, A. Alù, and J. B. Pendry, Adv. Opt. Photonics **4**, 014002 (2022).
[22] A. Sheikh Ansari, A. K. Iyer, and B. Gholipour, Nanophotonics **12**, 2639 (2023).
[23] T. Liu, C. Guo, W. Li, and S. Fan, eLight **2**, 25 (2022).
[24] S. Yang, M. Liu, C. Zhao, S. Fan, and C.-W. Qiu, Nat. Photonics **18**, 412 (2024).
[25] Y.-l. Ren, S.-l. Ma, J.-k. Xie, X.-k. Li, M.-t. Cao, and F.-l. Li, Phys. Rev. A **105**, 013711 (2022).
[26] J. Chen, H. Yu, and G. Gubbiotti, J. Phys. D **55**, 123001 (2022).
[27] S.-A. Biehs, R. Messina, P. S. Venkataram, A. W. Rodriguez, J. C. Cuevas, and P. Ben-Abdallah, Rev. Mod. Phys. **93**, 025009 (2021).
[28] S. Cardenas-Lopez, S. J. Masson, Z. Zager, and A. Asenjo-Garcia, Phys. Rev. Lett. **131**, 033605 (2023).
[29] S. Pucher, C. Liedl, S. Jin, A. Rauschenbeutel, and P. Schneeweiss, Nat. Photonics **16**, 380 (2022).
[30] M. Lawrence and J. A. Dionne, Nat. Commun. **10**, 3297 (2019).
[31] T. Peters, L. P. Yatsenko, and T. Halfmann, Phys. Rev. A **103**, 063302 (2021).
[32] See Supplemental Material at http://link.aps.org/supplemental/10.1103/9dhz-dxc8 for details regarding the TWA simulations and experiment, which includes Refs. [33–36].
[33] A. S. Sheremet, M. I. Petrov, I. V. Iorsh, A. V. Poshakinskiy, and A. N. Poddubny, Rev. Mod. Phys. **95**, 015002 (2023).
[34] G. Calajó and D. E. Chang, Phys. Rev. Res. **4**, 023026 (2022).
[35] P. T. Starkey, Ph.D. thesis, Monash University, Melbourne, 2019.
[36] D. Polder, M. F. H. Schuurmans, and Q. H. F. Vrehen, Phys. Rev. A **19**, 1192 (1979).
[37] G. Ferioli, I. Ferrier-Barbut, and A. Browaeys, Phys. Rev. Lett. **134**, 153602 (2025).
[38] C. Bach, F. Tebbenjohanns, C. Liedl, P. Schneeweiss, and A. Rauschenbeutel, Phys. Rev. Lett. **136**, 063402 (2026).
[39] M. S. Malcuit, J. J. Maki, D. J. Simkin, and R. W. Boyd, Phys. Rev. Lett. **59**, 1189 (1987).
[40] C. D. Mink and M. Fleischhauer, SciPost Phys. **15**, 233 (2023).
[41] H. T. Dung, L. Knöll, and D.-G. Welsch, Phys. Rev. A **66**, 063810 (2002).
[42] D. Dzsotjan, J. Kästel, and M. Fleischhauer, Phys. Rev. B **84**, 075419 (2011).
[43] T. Caneva, M. T. Manzoni, T. Shi, J. S. Douglas, J. I. Cirac, and D. E. Chang, New J. Phys. **17**, 113001 (2015).
[44] A. Asenjo-Garcia, J. D. Hood, D. E. Chang, and H. J. Kimble, Phys. Rev. A **95**, 033818 (2017).
[45] H. Pichler, T. Ramos, A. J. Daley, and P. Zoller, Phys. Rev. A **91**, 042116 (2015).
[46] F. Tebbenjohanns, C. D. Mink, C. Bach, A. Rauschenbeutel, and M. Fleischhauer, Phys. Rev. A **110**, 043713 (2024).
[47] C. D. Mink, D. Petrosyan, and M. Fleischhauer, Phys. Rev. Res. **4**, 043136 (2022).
[48] S. A. R. Horsley, J.-H. Wu, M. Artoni, and G. C. La Rocca, Phys. Rev. Lett. **110**, 223602 (2013).
[49] D.-W. Wang, H.-T. Zhou, M.-J. Guo, J.-X. Zhang, J. Evers, and S.-Y. Zhu, Phys. Rev. Lett. **110**, 093901 (2013).
[50] K. J. Kusmierek, M. Schemmer, S. Mahmoodian, and K. Hammerer, arXiv:2412.14930.
[51] Note that, different from [50], which discusses a related mechanism for emergent unidirectionality, the spatial separation between all emitters has the same uncertainty σ_z and does not accumulate.

End Matter

Static model with location uncertainty—To corroborate that the directionality and its dependence on N_{mc} and σ_{v} is due to motional-induced dephasing and the fact that the dipole transition matrix elements of the dressed two-level system [see Fig. 1(a)] have a space-dependent phase, we describe the effect of atomic motion by a static model with position uncertainty $z_l \to z_l + \xi_l$, where the ξ_l are random with $\overline{\xi_l} = 0$, $\overline{\xi_l^2} = \sigma_z^2$. Since the position uncertainty results from the motion of the atoms during the characteristic time τ of the collective coupling process, one has $\sigma_z = \bar{v}\tau$ [51]. The static model strictly applies only when the spatial phase factor of the effective dipole $\sim e^{ik_p z}$ changes substantially during the time τ. It nevertheless serves as an instructive toy model to explain the physical origin of the induced directionality of the collective emission. The dynamic TWA does not separate why κ is nonmonotonic in N_{mc}: there, the emission timescale is an emergent quantity and cannot be varied independently of the ensemble. In the static model, atomic motion enters only via the localization width σ_z, so τ sets the strength of the motional dephasing that controls the directionality and sets an explicit timescale. Averaging Γ_{lm}, J_{lm}, and $E_{\pm}$ over the spatial distribution creates an asymmetry in the coupling in $(\pm)$ direction, where $\beta_+ = \frac{1}{2}$ and $\beta_- = \frac{1}{2}\exp\{-[4\pi(\bar{v}\tau/\lambda_0)]^2\}$. Above, we have used $k_p \approx k_0 = 2\pi/\lambda_0$. Furthermore, the averaged emitted light intensity in the $(-)$ direction $I_- \sim \sum_{jl} \overline{e^{i(k_p+k_0)z_{jl}}} \langle \sigma_j^+ \sigma_l^- \rangle$ attains a term β_-^2 in the contributions with $j \neq l$, while I_+ remains approximately unchanged. Thus, for sufficiently large $\sigma_z = \bar{v}\tau$, collective emission into the $(-)$ direction is suppressed. This way, the static model maps the velocity distribution onto a location blur of width σ_z.

In Fig. 4(b), we also show two examples for TWA simulations of a static ensemble of atoms with effective couplings $\beta_\pm$ and $\sigma_{\mathrm{v}} = 3$. In the first example, a

representative constant $\tau = 0.019\Gamma^{-1}$ (open circles) is chosen to match the TWA at $N_{\mathrm{mc}} = 100$, and in the second, we use the characteristic superradiant time [2] $\tau(N_{\mathrm{mc}}) = (N_{\mathrm{mc}}\Gamma/2)^{-1}$ (full circles) (see Supplemental Material [32]). A constant τ neglects the fact that for increasing N_{mc} the collective timescale shortens. On the other hand, $\tau(N_{\mathrm{mc}})$ overestimates the impact of the varying collective timescale, i.e., the mapping's N_{mc} dependency. In absence of a precise theoretical prediction for τ, one could use a fit of the timescale for each N_{mc}, denoted as $\tau^*(N_{\mathrm{mc}})$, such that the static and the dynamic model agree. As anticipated by Fig. 4(b), the required weak but not vanishing N_{mc} dependency is closer to the constant τ than to $\tau(N_{\mathrm{mc}})$. The matched $\tau^*(N_{\mathrm{mc}})$ and a comparison to $\tau(N_{\mathrm{mc}})$ can be found in Fig. S1 of Supplemental Material [32].